Optics & Laser Technology 45 (2013) 533–539

Contents lists available at SciVerse ScienceDirect

Optics & Laser Technology

journal homepage: www.elsevier.com/locate/optlastec

Modeling and simulation of laser cleaning of tapered micro-slots with different temporal pulses

Liyang Yue [a,*], Zengbo Wang [a,b], Lin Li [a]

[a] Laser Processing Research Centre, School of Mechanical, Aerospace and Civil Engineering, University of Manchester, Sackville Street, Manchester M13 9PL, UK
[b] School of Electronic Engineering, Bangor University, Dean Street, Bangor, Gwynedd LL57 1UT, UK

ARTICLE INFO

Article history:
Received 15 April 2012
Received in revised form
17 May 2012
Accepted 30 May 2012
Available online 25 June 2012

Keywords:
Laser cleaning
Micro-slot
FEM

ABSTRACT

Thermal based laser surface cleaning could strongly depend on the temporal pulse shaping of laser. In this study, we have investigated, based on a Finite Element Method (FEM), the effects of different temporal pulses (Excimer laser, 248 nm, 26 ns), including rectangular and Gaussian shapes, in laser cleaning of microtapered slots covered by oil film (1.0 μm thick). The FEM model was verified with an analytical solution for a flat surface, and then applied to the tapered micro-slots structure. Plasma shielding effect as an important factor was included in current model. The temporal heating profiles with various laser fluences at different locations of micro-slot were obtained. Corresponding cleaning effects on the cross section of oil film were illustrated. Besides, a mesh size control equation was derived, which could ensure the modeling accuracy ($<3\%$ deviation). This work has laid down a theoretical base for further research work in laser cleaning of tapered micro-slots.

1. Introduction

Laser cleaning is a rapidly expanding subject within the laser material processing field in the last 20 years. It has been shown that pulsed laser cleaning is able to remove the contaminants from the various material surfaces and effectively protect the substrate from being damaged because of non-physical contact and precise control of the laser ablation depth [1–3]. This cleaning method was initially attempted to process the semiconductor material (silicon) by Tam and Zapka [4,5]. Their experiments indicated that various conformations of contaminants could be successfully cleaned by a pulsed laser. The ultraviolet light with wavelength of 248 nm irradiated by excimer laser provides higher emission current on the surface, which could enhance the cleaning effect [3]. Meanwhile, more and more laser cleaning tasks have been finished by nanosecond laser recently due to its outstanding short pulse duration. Compared with continuous wave or millisecond pulse lasers, nanosecond laser could provide higher peak power, furthermore boost the cleaning efficiency per pulse. Also, short pulse (ns pulse) and its low duty cycle could greatly restrict the expansion of heat affected zone on the cleaning target surface. For this reason, the substrate could be better protected from the heat damage [3]. Therefore, nanosecond laser has become the mainstream of equipment in laser cleaning field, and many achievements are obtained by previous researchers [6–8]. On the other hand, tapered silicon micro-slot is a common structure in chemical etching of silicon wafer, and has been widely used in semi-conductor industry [9,10]. In the mass production, the silicon wafers could be sealed by a thin layer of oil as in fabricating of the 3D micro-gears or the microelectromechanical systems (MEMS) devices, which could be the residue that adheres on the tapered micro-slot after chemical etching [11,12]. Despite the work by Lee et al. on laser cleaning of plasma-etching-induced polymer residuals in 800 nm deep hole [13], there has been no report on laser cleaning of tapered micro-slots.

During the laser cleaning process, high energy densities provided by pulsed laser provoke abrupt heating–cooling cycles. Material absorption of the laser energy and corresponding heating on the surface could be mathematically expressed by the heat conduction differential equations with either analytical or numerical solutions [14–17]. The temporal shapes of laser play an important role and the thermal history of the material is significantly influenced by it. Compared with analytical solutions, FEM (numerical) is applied to complex geometry. Its calculation progress is theoretically expressed as a numerical approach of partial differential equations (PDE) using integral equations and proper boundary conditions [18]. The established literatures proved that plasma shielding effect should be concerned in the simulation of laser processing involving high intensity laser beam vaporisation of materials, because a large amount of electrons, ions and excited neutrals coexisting would absorb the laser energy and form a plasma cloud above the target surface, which

* Corresponding author. Tel.: +44 750 3920477.
E-mail address: liyang.yue@postgrad.manchester.ac.uk (L. Yue).

0030-3992/$ - see front matter © 2012 Elsevier Ltd. All rights reserved.
http://dx.doi.org/10.1016/j.optlastec.2012.05.036

may partially or fully block the energy input from the laser beam [19,20].

In this paper, a mesh size control equation was initially derived and an FEM model was developed based on two temporal beam shapes (rectangular and Gaussian). This was verified with established analytical solution for a flat surface model. Comprehensive modeling of laser cleaning of tapered micro-slot layered oil film was consequently carried out after the above verification. The optical thickness of plasma cloud was assumed to evenly increase during the pulse duration, and had uniform absorptivity for the laser energy. Corresponding temporal heating profile and cleaning effect on the cross section of the oil film were illustrated. Material phase change, reflectivity changes at locations and temperature dependent material properties were taken into account in the modeling.

2. Numerical simulation

2.1. Boundary conditions

There are three types of heat transfers involved in the laser heating model: conduction, convection and radiation. The absorbed laser light energy changes into thermal energy at the laser material interaction zone on the substrate surface, and the temperature would rise above the melting point of the material. Then phase change occurs immediately. The heat flow process involved is dominated by conduction [21]. In this period, some of the heat in the melt pool may be lost to environment in the electromagnetic wave form, which is called radiation heat transfer, and does not require the presence of a medium. Thermal convection interaction describes the thermal energy in laser beam-material interaction zone dispersed by the influence of environmental fluid flow [22]. Considering the short pulse duration and high peak power for nanosecond laser, thermal convection and radiation only take small proportion of energy diffusion in bulk of material, which is neglected in current model [23]. The thermal conduction is the only formation of heat transfer chosen in ANSYS software. Thus, several assumptions are ensured in this paper.

(1) All entities in this model are defined as homogeneous bodies, and corresponding thermal properties are isotropic.
(2) Laser beam intensity distribution is an ideal flat top beam. The loaded power intensity in the beam irradiation area is constant.
(3) The power loss in the form of convection and radiation are neglected. The thermal conduction is the only formation of heat transfer in this model.
(4) The multiple reflection that would happen inside micro-slot is neglected. All reflectivities used this model is based on the wavelength 248 nm.
(5) The sublimation and recoil pressure of material is ignored in this model. The phase change follows the classic solid–liquid–vapor order, and the energy consumed during this process is represented by the enthalpy of material.

Following heating process and boundary conditions are described by Eqs. (1)–(4) [24].

$$\rho(T)C(T)\partial T(r,t)/\partial t = \nabla[k(T)\nabla T(r,t)] \quad T_0 < T < T_{bp} \tag{1}$$

$$\frac{\partial H(T)}{\partial t} = \nabla\left[k\nabla T(r,t)\right] \quad T \geq T_{bp} \tag{2}$$

$$-k\frac{\partial T}{\partial z_{z=0}}\Big| = I\left(\vec{r},t\right) \quad \text{on surface,} \quad t > 0 \tag{3}$$

$$T(\vec{r},0) = T_0 \quad t = 0 \tag{4}$$

where ρ is the density, C is the heat capacity, t is the time, r is the radial position, $H(T)$ is the enthalpy function that incorporates the phase changes of the material, k is the thermal conductivity, z is the depth, T is the temperature field, T_{bp} is the boiling point, T_0 is the ambient temperature, I is the laser beam intensity distribution which can be expressed by space and time domains equations. All differential equations of laser irradiation on the solid surface are calculated in the non-linear solution mode [25].

2.2. Modeling geometry and reflectivity

The model geometry consists of a 1.0 μm thick uniform oil film covering a tapered micro-slot structure. The taper angle was 10°. Fine element (side length < 50 nm) was employed to mesh the oil film part to elevate the accuracy. The schematic and dimensions are shown in Fig. 1(a). Two reflectivities are involved to distinguish the locations of the slot (top surface, bottom and side walls). The reflectivity of the oil was 0.048 for the top surface and the bottom and 0.397 for the side walls. The reflectivities of silicon were to 0.675 (top surface and bottom) and 0.687 (side walls) [26,27].

2.3. Temporal pulse shapes

Rectangular and Gaussian pulses were separately loaded. The intensity of single rectangular pulse can be expressed by [17],

$$I_0(t) = I_0 H(\tau_\ell - t)H(t) \tag{5}$$

where $I_0(t)$, I_0, H and τ_ℓ are intensity of incident laser, the maximum intensity, Heaviside function and pulse duration

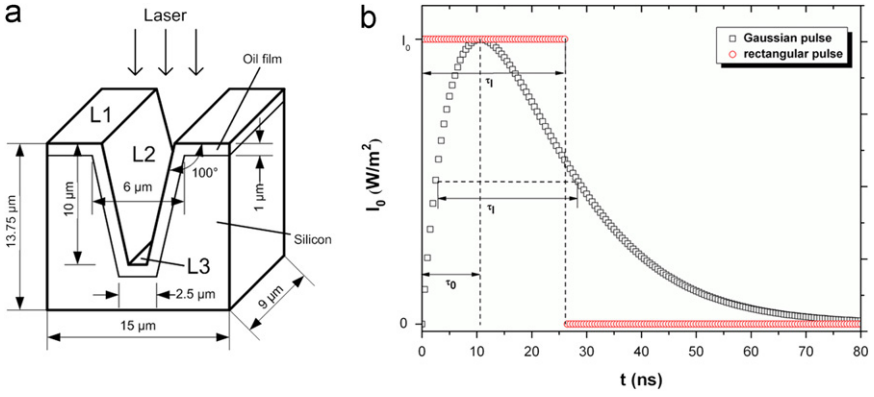

Fig. 1. (a) The dimension of micro-slot structure and (b) temporal variation of the intensity for rectangular and Gaussian pulses.

respectively. The laser fluence, ϕ_R, for this pulse is:

$$\phi_R = I_0 \tau_\ell \tag{6}$$

Meanwhile, the intensity of the Gaussian pulse is given by following equation [17],

$$I_0(t) = I_0 \left(\frac{t}{\tau_0}\right)^{\beta} \exp\left[\beta\left(1-\frac{t}{\tau_0}\right)\right] \tag{7}$$

where β describes the temporal shape factor, and τ_0 is the duration that intensity increases to the maximum value from 0. The expression of fluence, ϕ_G, for Gaussian pulse is defined as [17],

$$\phi_G = I_0 \tau_0 \exp(\beta) \frac{\Gamma(\beta+1)}{\beta^{\beta+1}} \tag{8}$$

Here the shape factor β is set to 1, $\Gamma(\beta+1)$ represents the gamma function which equals to the factorial of β here. The relationship between $\tau_\ell$and τ_0 can be obtained by Eq. (7), approximately as $\tau_\ell = 0.409\,\tau_0$. For comparison, the aforementioned two pulse shapes were calculated for the same fluence, $\phi_R = \phi_G$, which makes their integrations with the same squares on the intensity shape, as shown in Fig.1(b).

2.4. Material properties

The energy consumed by phase change has taken into account the material properties and reflects on the temperature dependence of enthalpies. All the temperature dependent and constant properties of crystalline silicon and oil irradiated by the excimer laser (248 nm wavelength) are given in Tables 1 and 2 [28,29]. T_{mp} and A represent the melting point and absorptivity respectively in the tables.

2.5. Mesh element

To attach the temperature dependent enthalpies non-linear solution method is selected. For this reason, convergence conditions have become stricter than linear solution mode, which can easily lead to non-convergence on the mesh elements with a high node number. Considering the calculation speed and uneven meshing on the interface between oil film and silicon substrate, pyramid elements with 5 nodes were applied.

Table 1
Material properties of crystalline silicon [28,29].

ρ (kg/m^3)	2320	T_{mp} (°C)	1414		T_{bp} (°C)	3265		A	0.325
T (°C)	27	227	427	727	927	1227	1412	1727	2227
H (J/cm^3)	3.286	354.9	727.1	1320	1739	2406	2842	8213	9537
k (W/m K)	148	76.2	51	31.2	25.7	22.5	22	20	18
C (J/kg K)	705	830	860	880	910	920	925	930	930

Table 2
Material properties of oil film [28,29].

ρ (kg/m^3)	860	T_{mp} (°C)	−10	T_{bp} (°C)	280	A	0.95
T (°C)	0	37		54.8	67.9		82.5
H (J/cm^3)	214.2	241		276	298		327
k (W/m K)	0.18	0.17		0.15	0.15		0.13
C (J/kg K)	1680	1700		1780	1900		2090

2.6. The plasma shielding effect

The mechanism of material ionisation is sophisticated and strongly affected by many factors including material properties, concentration and thickness of plasma electrons and the ion cloud. However, for calculation purpose a simplified model is established based on Beer–Lambert law, which assumes that a layer of plasma contacts the evaporation face closely. Its expression is given as [30],

$$I_s(t) = I_0(t)\exp(-\alpha \Lambda) \tag{9}$$

where $I_s(t)$ is the temporal laser intensity at the sample surface, α is absorption coefficient of plasma cloud, Λ is the thickness of plasma cloud. The thickness of plasma cloud, Λ, is given by [31],

$$\Lambda = c_s t \quad 0 < t < \tau_\ell \tag{10}$$

where c_s is the hydrodynamic expansion velocity of the plasma, which approximates to 340 m/s. The absorption coefficient α is deduced from the Eq. (11), which is expressed by [32]

$$\alpha = \frac{4\pi k_{ext}}{\lambda} \tag{11}$$

where k_{ext} and λ are extinction coefficient of material and wavelength of laser, respectively. From the established literature, it is known that absorption coefficient is also related to the laser output power [33]. In this case, absorption coefficient, α, is assumed as 4.23×10^4/m.

3. Results and discussion

3.1. Mesh size

In the course of building the current model, it was found that the side length of the mesh element, l, should be smaller than the state diffusion of the material, which ensures that boundary conditions could link each node and be loaded on the individual element for the best accuracy. The schematic of pyramid mesh element and its side length are illustrated in inset in Fig. 2(a). The equations of diffusivity, D, is given by [34],

$$D = \frac{k}{\rho C} \tag{12}$$

where D is the thermal diffusivity.

The state diffusion, J, is expressed by

$$J = G\sqrt{D\tau_\ell} \tag{13}$$

where J and G are the state diffusion and empirical factor respectively. The empirical factor G could further improve the accuracy of the model. In this case, considering the calculation time, the empirical factor G is derived to be 0.9 through the practical comparison of the temporal rise curves for multiple values. Due to the fact that the thermal conductivity of the oil film is low, the state diffusion of oil, J, is only 54.9 nm based on Eqs. (12) and (13). Therefore, the side length of the mesh element should be below this value, and all the numerical solution in this paper are based on the geometry meshed by the element whose side length is below 50 nm. The analytical solution of rectangular pulse laser heating substrate is used to verify aforementioned rule [17], and the curves using the multiple mesh sizes are also involved, as shown in Fig. 2(a). The black curve in Fig. 2(a) is the standard analytical heating curve. It is found that the curve for $l < J$ (red) is much closer to the result of the analytical solution than the curves for the other mesh sizes.

3.2. Flat surface model

A flat surface model ($z=0$) is established to verify the feasibility of FEM (numerical) model from the proportions of peak temperature and peak temperature time between rectangular and Gaussian pulses on temporal heating profiles. Fig. 2(b) shows the temporal heating profiles initiated by the rectangular and Gaussian laser pulses with the same fluence solved by the numerical (dot line) and the analytical (solid line) methods. The analytical profile is obtained from the established literature [17]. Its analytical proportions between two pulse shapes are defined as the criterion, which would be compared with that for numerical solution. The normalised peak temperature and peak temperature time for the rectangular pulse are set to 1.0 in Fig. 2(b). The FE modeling result is plotted and compared to the analytical one. Plasma shielding effect is temporarily ignored from the FEM model for the objective comparison with the established literature under the same modeling conditions.

Fig. 2(b) shows that the temporal heating profiles and corresponding proportions calculated by two methods are in good agreement. It is observed that the result of the temperature profiles for the rectangular laser pulse calculated by the FE (numerical) model nearly coincides to the analytical one, and is only slightly higher during the cooling period. For the analytical curves (solid lines) the normalised peak temperature and peak temperature time of Gaussian pulse are 0.67 and 0.92 respectively. However, the peak temperature calculated by the numerical solution is higher than these values reaching, 0.70, and a 3% discrepancy appears. The main reason for this could be the error of enthalpy values used in the non-linear solver [35]. Therefore, the FE model is verified to be able to provide a reasonable result for the simulation of laser cleaning with rectangular and Gaussian pulses and the modeling error is low.

3.3. Tapered micro-slot modeling

The FE model simulation is that plane wave laser beam (248 nm, 26 ns) vertically irradiating on the micro-slot structure. The geometry has three parts: top surface (L1), side walls (L2) and the bottom surface (L3), as shown in Fig. 1(a). The ambient temperature is set to 20 °C. Fig. 3 shows that the temporal heating profiles on the oil film surface ($z=0$) irradiated by rectangular and Gaussian pulses with 5 fluences (30, 40, 50, 60 and 70 mJ/cm^2) at three locations (L1, L2 and L3). Theoretically the oil film where temperature is below the boiling point ($T_{bp}=280$ °C, as shown in Fig. 3) directly absorbs the energy from the laser and maintains its liquid state. When its temperature is above the boiling point, the phase change occurs immediately. The oil film starts transferring into the plasma cloud that travels away from the surface towards the laser beam. Meanwhile, the plasma cloud replaces the oil film and absorbs the laser energy. Its temperature and thickness would increase rapidly because of plasma shielding effect during the pulse duration of nanosecond laser [36]. Therefore, the temperature above the boiling point is the plasma cloud temperature in Fig. 4. Also, the oil film where temperature is above the boiling point is considered to be cleaned from substrate.

Fig. 3 (1–6) indicates that the peak temperatures on the heating profiles are linear to the increase of laser fluences. The curves of 70 mJ/cm^2 have the highest peak temperature, as shown in Fig. 3 (1–6). For the curve with the same fluence and location it is found that the peak temperature of rectangular pulse approximates 29% higher than that for the Gaussian pulse. The peak temperatures for the rectangular and the Gaussian pulses occur at 26 ns and 24 ns respectively. Also, for both the rectangular and Gaussian pulses it is observed that the temperature rise of the side wall (L2) is far lower than those on the top surface and the bottom of the slot. Its peak temperature on the side wall is only about 10% of those on the other locations (L1 and L3) with the same fluence, because the side walls (L2) have the smaller horizontal projection and lower beam intensity. Meanwhile, the 3D temperature distribution of 40 mJ/cm^2 for Gaussian shape at 10 ns is illustrated in Fig. 3 (7). The distributions for other fluences are similar to it.

The cleaning depth and temperature distribution on the cross section of the oil film for the rectangular and Gaussian pulses with 70 mJ/cm^2 are shown in Fig. 4. The smaller mesh size (15 nm) is employed for the illustration of temperature distribution of oil film after laser irradiation. The elements where the temperature is above the boiling point of oil are removed. From Fig. 4, it is known that the cleaning depths for the rectangular pulse are 130 nm (L1), 50 nm (L2), and 135 nm (L3) respectively, and for the Gaussian pulse, the depths are 115 nm (L1), 40 nm (L2) and 120 nm (L3) respectively.

Meanwhile, Fig. 5 describes the cleaning depth of rectangular and Gaussian pulses as a function of fluence (20 mJ/cm^2, 30 mJ/cm^2, 40 mJ/cm^2, 50 mJ/cm^2, 60 mJ/cm^2, 70 mJ/cm^2, 80 mJ/cm^2, and 90 mJ/cm^2) at three locations (L1, L2 and L3). It is clear that for the same location the cleaning depth is linear to the increase of fluence. For the same location and fluence it is observed that rectangular pulse could provide higher cleaning depth compared with that of the Gaussian pulse. The difference between them is from 10 nm to 20 nm. Also, it is found that the cleaning depth of

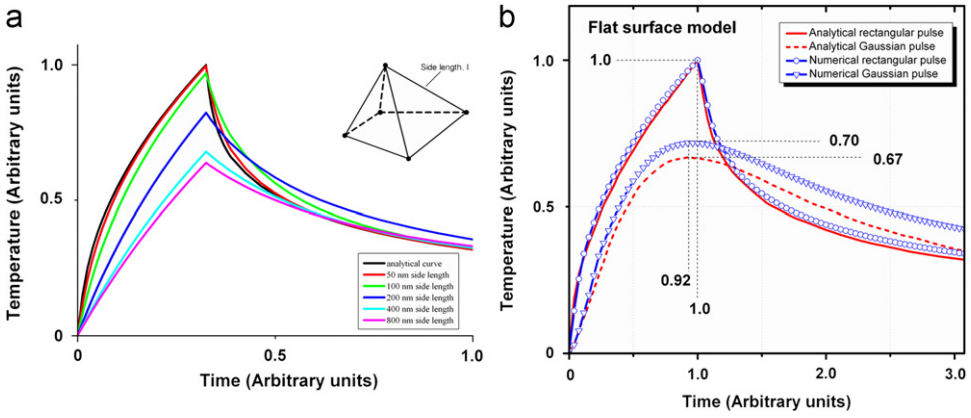

Fig. 2. (a) Temperature profiles calculated by the analytical solution and numerical solution using FE modeling with multiple mesh sizes and (b) temporal temperature profiles on a flat surface irradiated by the rectangular and Gaussian pulses with the same fluence. Solid and dot lines are calculated by analytical and numerical solution respectively. (For interpretation of the references to colour in this figure legend, the reader is referred to the web version of this article.)

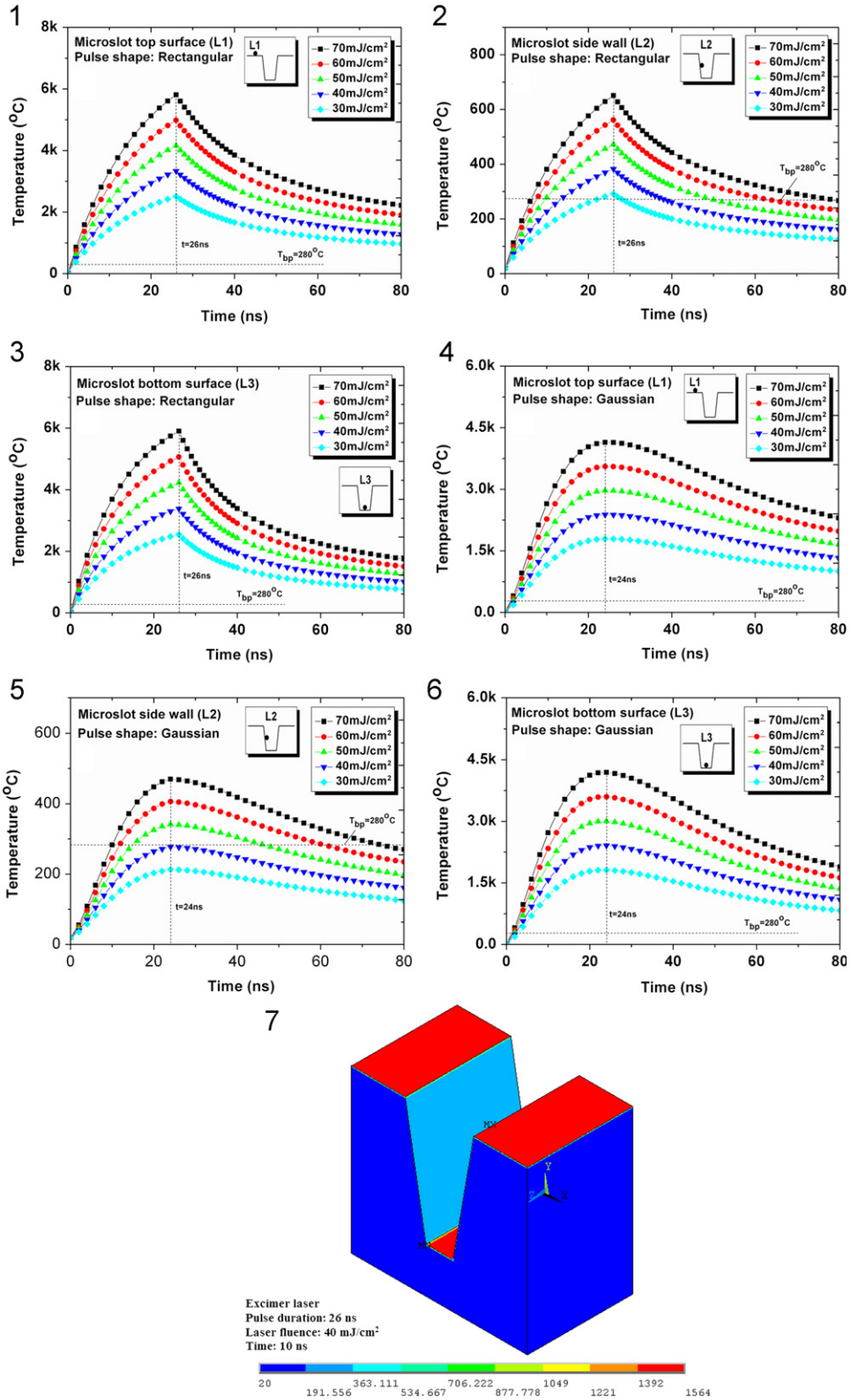

Fig. 3. Temporal heating profiles of at top surface (L1), side wall (L2) and bottom (L3) with multiple laser fluence for (1–3) rectangular and (4–6) Gaussian pulses. The 3D temperature distribution of 40 mJ/cm^2 for Gaussian shape at 10 ns is illustrated in (7).

side walls (L2) is much lower than the other two locations under the same laser parameters. The cleaning depth can drop to 0 at low fluences, as shown in Fig. 5. The cleaning threshold is the minimum input laser energy density required to remove the contaminant. The cleaning thresholds of tapered micro-slot structure depend on the cleaning depth at side walls (L2) and can be predicted by the current model. All the predicted cleaning thresholds for rectangular and Gaussian pulses are presented in Table 3. It shows that higher fluences and extra pulse number are required for the cleaning of side walls (L2). In addition, the

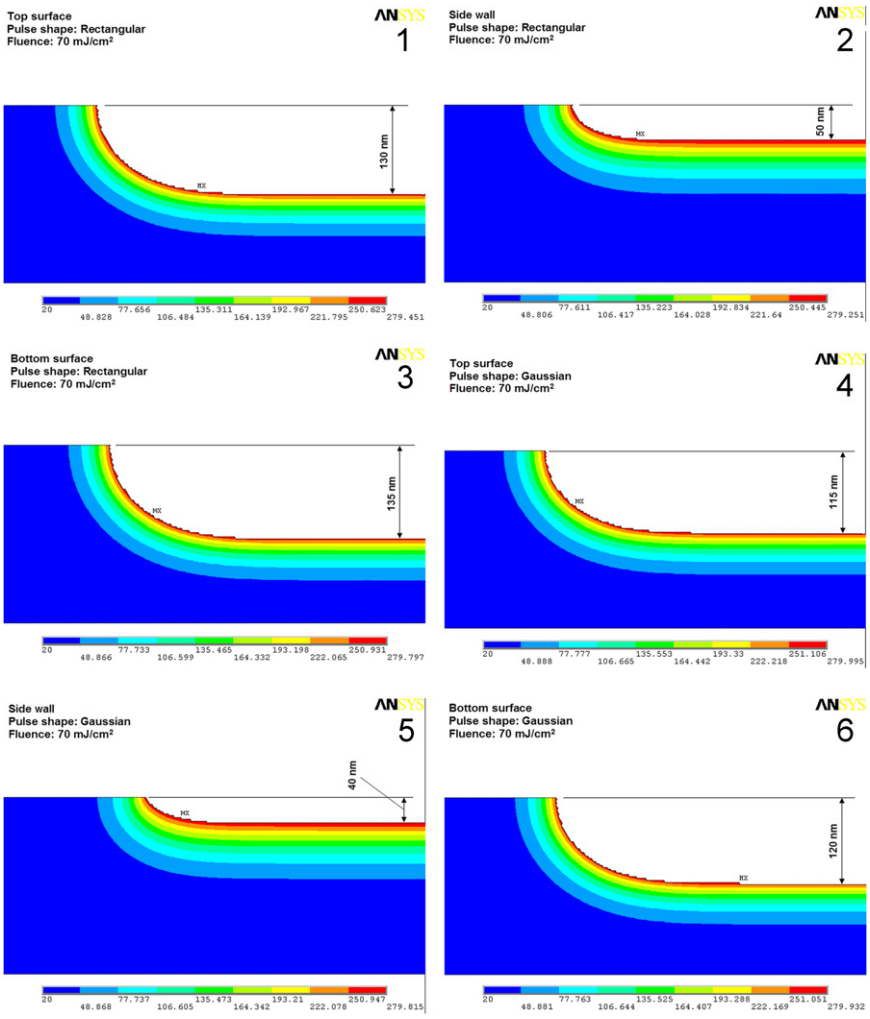

Fig. 4. The cleaning depths and temperature distributions on the cross section of oil film at top surface (L1), side wall (L2) and bottom (L3) for (1–3) rectangular and (4–6) Gaussian pulses.

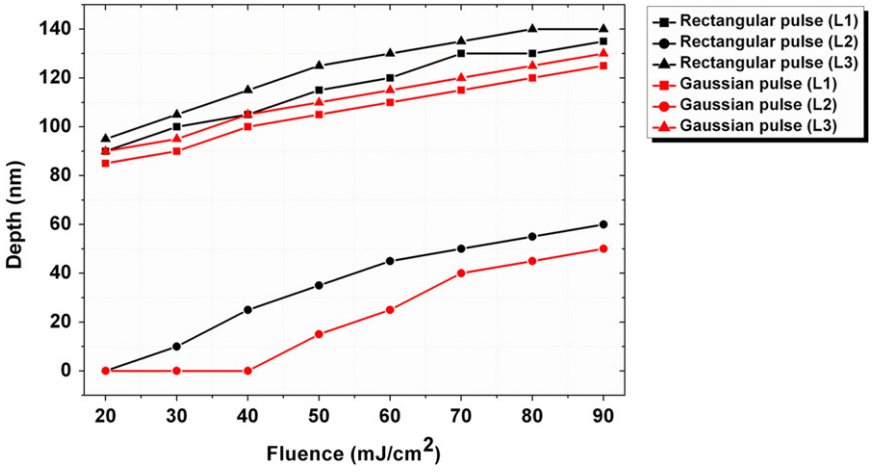

Fig. 5. The Cleaning depths of the rectangular and Gaussian pulses as a function of laser fluence (20 mJ/cm^2, 30 mJ/cm^2, 40 mJ/cm^2, 50 mJ/cm^2, 60 mJ/cm^2, 70 mJ/cm^2, 80 mJ/cm^2, and 90 mJ/cm^2) at three locations (L1, L2 and L3).

cleaning depth on bottom surface is larger than that on top surface, and the average difference is about 10 nm.

The phenomenon that rectangular pulse provides higher peak temperature and larger cleaning depth could be caused by two factors. Firstly, the rectangular pulse could keep the maximum power intensity, I_0, for the whole pulse duration (26 ns), which benefits the accumulation of energy on the substrate surface. Reversely, although Gaussian pulse has longer pulse output time, it only achieves to the peak intensity at time, τ_0, and then the power intensity starts to go down, as shown in Fig. 1(b). It is known that the amount of energy provided by Gaussian pulse would be smaller than that of rectangular pulse in the unit laser

Table 3
The cleaning thresholds on micro-slot model.

Temporal laser pulse	Cleaning threshold (mJ/cm^2)
Rectangular	20
Gaussian	40

output period. Secondly, as the main formation of thermal transfer, thermal conduction continuously influences the temperature rise at the substrate surface. Compared with the laser power intensity absorbed by material surface, the intensity loss led by thermal conduction at surface only takes the small proportion of power intensity input in whole system which is less than 1% in this case based on Eq. (3). The intensity loss could offset part of the input laser intensity on the material surface. For the rectangular pulse its working period is only the pulse duration (26 ns), which is far shorter than that for Gaussian pulse. Therefore, more laser fluence would be offset due to thermal conduction if Gaussian pulse is employed in cleaning task.

4. Conclusion

The FE model successfully simulates the laser cleaning of tapered micro-slot structure irradiated by temporal rectangular and Gaussian pulses, and the cleaning thresholds are predicted based on it. A mesh size control equation has been derived, which provides the modeling accuracy ($< 3\%$ deviation) compared with established analytical solution. The micro-slot model indicates that the rectangular pulse has higher cleaning efficiency compared to the Gaussian pulse, and cleaning depth at side walls (L2) is lower than the other locations (L1 and L3) using the same laser parameters.

Acknowledgement

Part of the research was financially supported by the Engineering and Physical Science Research Council (EPSRC), Grant no. EP/G034745/1 within the SAMULET programme.

References

[1] Lu YF, Sung WD, Hong MH, Teo BS, Chong TC, Low TS. Laser removal of particles from magnetic head sliders. Journal of Applied Physics 1996;80:499–504.
[2] Lu YF, Takai M, Komuro S, Shiokawa T, Aoyagi Y. Surface cleaning of metals by pulsed-laser irradiation in air. Applied Physics A 1994;59:281–8.
[3] Lukyanchuk BS. Laser cleaning. Singapore: World Scientific; 2002 pp. 27–430.
[4] Zapka W, Tam AC, Ziemlich W. Laser cleaning of wafer surfaces and lithography masks. Microelectronic Engineering 1991;13:547–50.
[5] Tam AC, Leung WP, Zapka W, Ziemlich W. Laser cleaning techniques for removal of surface particulates. Journal of Applied Physics 1992;71:3515–23.
[6] Mosbacher M, Chaoui N, Siegel J, Dobler V, Solis J, Boneberg J, et al. A comparison of ns and ps steam laser cleaning of Si surfaces. Applied Physics A 1999;69:S331–4.
[7] Dobler V, Oltra R, Boquillon JP, Mosbacher M, Boneberg J, Leiderer P. Surface acceleration during dry laser cleaning of silicon. Applied Physics A 1999;69:S335–337.
[8] Arnold N. Theoretical description of dry laser cleaning. Applied Surface Science 2002;208–209:15–22.
[9] de Boer MJ, Gardeniers JGE, Jansen HV, Smulders E, Gilde MJ, Roelofs G, et al. Guidelines for etching silicon MEMS structures using fluorine high-density plasmas at cryogenic temperatures. Journal of Microelectromechanical Systems 2002;11:385–401.
[10] Bhardwaj JK, Ashraf H. Advanced silicon etching using high density plasma. Proceedings of SPIE 1995;2639:224–33.
[11] Yang C, Leong K. Influences of substrate wettability and liquid viscosity on isothermal spreading of liquid droplets on solid surfaces. Experiments in Fluids 2002;33:728–31.
[12] Korvink JG, Paul O. MEMS: A practical guide to design, analysis, and applications. Basel: Birkhauser; 2006 pp. 567–667.
[13] Lee YP, Lu YF, Chan DS, Low TS, Zhou MS. Steam laser cleaning of plasma-etch-induced polymers from via Hole. Japanese Journal of Applied Physics 1998;37:2524–9.
[14] Singh RK, Narayan J. Pulsed-laser evaporation technique for deposition of thin films: Physics and theoretical model. Physical Review B 1990;41:8843–59.
[15] Oliveira V, Vilar R. Finite element simulation of pulsed laser ablation of titanium carbide. Applied Surface Science 2007;253:7810–4.
[16] Vasantgadkar NA, Bhandarkar UV, Joshi SS. A finite element model to predict the ablation depth in pulsed laser ablation. Thin Solid Films 2010;519:1421–30.
[17] Bauerle D. Laser processing and chemistry. Berlin: Springer; 2000 pp. 106–114.
[18] Pelosi G. The finite-element method. Part I: R.L. Courant: Historical Corner, Antennas and Propagation Magazine, IEEE 2007;49:180–2.
[19] Fang R, Zhang D, Li Z, Yang F, Li L, Tan X, et al. Improved thermal model and its application in UV high-power pulsed laser ablation of metal target. Solid State Communications 2008;145:556–60.
[20] Singh RK, Viatella J. Estimation of plasma absorption effects during pulsed laser ablation of high-critical-temperature superconductors. Journal of Applied Physics 1994;75:1204–6.
[21] Tritt TM. Thermal conductivity: theory, properties, and applications. Berlin: Springer; 2004 pp. 1–17.
[22] Baierlein R. Thermal physics. Cambridge: Cambridge University Press; 1999 pp. 244–378.
[23] Chen MF, Wang YH, Hsiao WT. Finite element analysis and verification of laser marking on eggshell. Journal of Materials Processing Technology 2009;209:470–6.
[24] Ozisik MN. Heat conduction. New York: John Wiley & Sons; 1980 pp. 1–37.
[25] ANSYS Inc. Modeling and Meshing Guides. USA; 1998.
[26] Birkhoff RD, Painter LR, Heller JM. Optical and dielectric functions of liquid glycerol from gas photoionization measurements. Journal of Chemical Physics 1978;69:4185–8.
[27] Palik ED. Handbook of optical constants of solids. Boston: Academic Press; 1985 pp. 155–185.
[28] Chase MW. NIST-JANAF thermo-chemical tables. 4th ed. USA: The American Chemical Society and the American Institute of Physics; 1998 pp. 1881–1887.
[29] Zhelezny VP, Nichenko SV, Semenyuk YV, Skripov PV. Experimental investigation of enthalpy of isobutene-compressor oil solutions. Journal of Chemical and Engineering Data 2010;55:1322–6.
[30] Bulgakov AV, Bulgakova NM. Thermal model of pulsed laser ablation under the conditions of formation and heating of a radiation-absorbing plasma. Quantum Electronics 1999;29:433–7.
[31] Stafe M, Negutu C, Popescu IM. Theoretical determination of the ablation rate of metals in multiple-nanosecond laser pulses irradiation regime. Applied Surface Science 2007;253:6353–8.
[32] Ingle JD, Crouch SR. Spectrochemical analysis. Englewood Cliffs, New Jersey: Prentice Hall; 1988 pp. 372–381.
[33] Fabre E, Stenz C. CO_2-laser-beam absorption by a dense plasma. Physical Review Letters 1973;32:823–6.
[34] Lide DR. Handbook of chemistry and physics. 90th ed. Boca Raton: CRC Press; 2009 pp. 2–65.
[35] Conde JC, Gonzalez P, Lusquinos F, Chiussi S, Serra J, Leon B. Analytical and numerical calculations of the temperature distribution in Si and Ge targets irradiated by excimer lasers. Applied Surface Science 2005;248:455–60.
[36] Singh RK, Narayan J. Pulsed-laser evaporation technique for deposition of thin films: physics and theoretical model. Physical Review B 1990;41:8843–59.